Journal of
Materials Chemistry B

Accepted Manuscript

ROYAL SOCIETY
OF CHEMISTRY

www.rsc.org/materialsB

Journal of Materials Chemistry B

PAPER

Magnetically Triggered Drug Release from Biocompatible Microcapsules for Potential Cancer Therapeutics

Hongmei Bi[a,b] , Shenghua Ma[a], Qingchuan Li[a] and Xiaojun Han[a]*

This paper demonstrated that magnetic field triggered drug release from magnetic lipid microcapsules (MLMs) in a controlled manner. Two types of MLMs were fabricated, i.e., MLMs with negatively charged magnetic nanoparticles (MNPs) inside and MLMs with positively charged MNPs on their surfaces. The carboxyfluorescein (CF) and chemotherapy drug doxorubicin (Dox) release induced by AC magnetic field (AMF) were investigated in detail both experimentally and theoretically. Although the drug releases of these two types MLMs both synchronize the switch of AMF, they exhibited different mechanisms. The magnetic heating effect dominates the release of MLMs with MNPs inside, while both magnetic heating and oscillation effects play important roles for the release of MLMs with MNPs on the surfaces. The *in vitro* cytotoxicity experiments of Dox loaded microcapsules toward HeLa cells were further performed, which confirmed these magnetic responsive drug carries had obvious effect on cell apoptosis triggered by external non-invasively AMF.

1 Introduction

The development of controlled drug delivery by external stimuli has received tremendous attention in recent years. It has significant potential in targeted drug delivery through effective drug release at target regions.[1, 2] External stimuli, exploited for such applications, include pH,[3-5] temperature,[6] light,[7-9] magnetic-field,[10-12] and ultrasound.[13, 14] Among all stimuli, low strength magnetic field is considered as a promising tool to amplify drug efficacy in clinical treatment with minimum adverse effects because the magnetic field can easily penetrate the human tissues. Different materials were used to fabriate magnetic drug carriers together with ferroferric oxide nanoparticles. The composite polyelectrolyte capsules possessing magnetic filed controlled drug release function were developed recently for cancer therapy.[15, 16] Except polymer, gel were commonly used in this field,[17-19] some inorganic materials were also designed to fabriate magnetic drug carriers. Carbon nanotubes and mesoporous silica were served as templates for the fabrication of the magnetic silica carriers.[20, 21] The obtained hollow nanostructures consisting of magnetic nanoparticles were loaded with drug and used to remotely control the release of small molecules and drugs in response to an alternating magnetic field.[21] The membrane based materials were also exploited for controlled drug delivery. Nanocomposite membranes containing thermo responsive nanogels and superparamagnetic nanoparticles were demonstrated to provide on-off drug release upon application of an oscillating magnetic field. Hybrid beads composed of MNP and alginate were synthesized. The release of dopamine was also evaluated in the presence of external magnetic field.[22] Magneto-liposomes have recently been attracting attention for drug release due to the excellent biocompatibility.[11, 23, 24] The concept of magneto-mechanical actuation of single-domain MNPs in super-low and low frequency AMF was proposed.[25] The challenges and advancements of MNPs and nanocomposites for remote controlled therapies were discussed.[26,27] Although few investigations have been reported on exploiting magneto-liposomes in dye or drug release, the release mechanism of these systems was not fully clarified.

Herein, two types MLMs were fabricated for a direct observation of the drug release. A mimic drug and truth anti-cancer drug were entrapped in the internal lumen of the capsules to study the release process in AFM. We demonstrated the negatively charged MNPs were encapsulated into lipid microcapsules (LMs) (Fig.1a), and positively charged MNPs were absorbed onto the surface of LMs (Fig. 1c), which showed different drug release behaviours upon applying AMF. Their release mechanisms were investigated by computing simulations. Magnetic heating effect is mainly responsible for the negatively charged MNP loaded LMs, while both magnetic heating and magnetic oscillations effects contribute to drug release from positively charged MNPs loaded LMs. Furthermore the doxorubicin (Dox) loaded MLMs showed significant cytotoxicity towards Hela cells *in vitro*, which shows great potential in controlled drug release for treating cancer diseases.

a. State Key Laboratory of Urban Water Resource and Environment, School of Chemical Engineering and Technology, Harbin Institute of Technology, Harbin 150001, China.
b. College of Science, Heilongjiang Bayi Agricultural University, Daqing 163319, China.
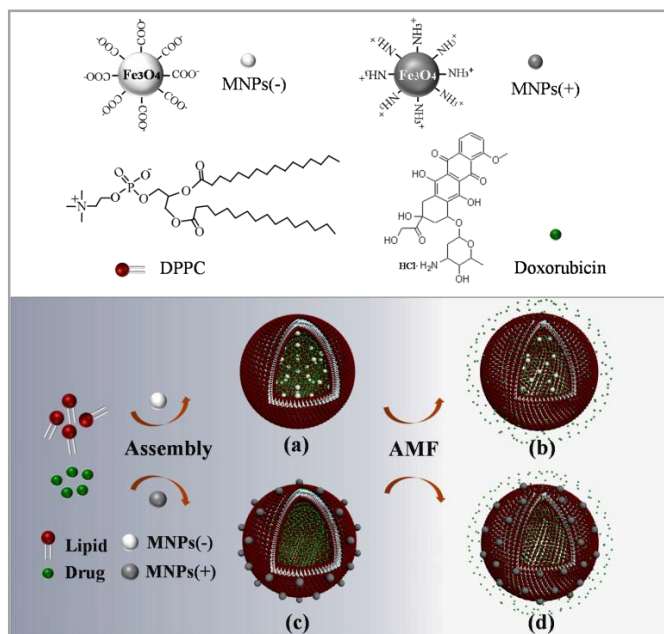
Fig.1 Schematic illustration of negatively charged MNPs and drug loaded LMs (a) and drug release (b) upon alternative magnetic field, and positively charged MNPs and drug loaded LMs (c) and drug release (d) upon AMF. Not to scale.

2 Experimental section

2.1 Synthesis of the Magnetic and Fluorescent LMs

MLMs were prepared using the electro-formation method.[28] Two ITO-coated microscope slides were used as formation electrodes due to the good transparency. ITO electrodes coated with lipid thin films were separated by a rectangular polytetra-fluoroethylene (PTFE) spacer with a length and width of 17 and 6 mm, respectively. The height was 2 mm (Fig. S1). Lipid solution (5.0 mg/mL), composing of DPPC (or DOPC) and TR-DHPE at a 99.5:0.5 mass ratio, was prepared in chloroform. Lipid thin films were prepared on two ITO electrodes using the flat-coating method as mentioned in details elsewhere.[29, 30] Briefly, 5 µL lipid solution was deposited onto ITO electrode surface using a needle to spread carefully back and forth for 5 times. Uniform lipid films were prepared and followed by drying under vacuum for 2 h. The chamber was then filled with 300 µL sucrose solution containing certain concentration of MNPs and 0.05 mg/mL CF (or 0.1 mg/mL Dox). AC electric field (sinusoidal wave with a frequency of 10 Hz and amplitude of 5 V) was applied for ~3 h to generate LMs. Then the capsules solution was gently removed from the chamber and filtered with polycarbonate membrane (400 nm) to wash out the particles and CF (or Dox) not entrapped in microcapsules.

2.2 The Release of CF or Dox from MLMs Triggered by an AC Magnetic Field

The encapsulated fluorescence dye, CF (excitation 492 nm, emission 517 nm, 0.05 mg/mL, 5.5×10^7 CF/LMs) or drug Dox (excitation 488 nm, emission 575 nm, 0.1 mg/mL, 4.2×10^7 Dox/LMs) were used as indicators to monitor the contents release from MLMs by the fluorescence intensity measurement

upon applying an AC magnetic field. The sample solutions (200 µL) (1.2×10^6 MLMs per mL, the average diameter of LMs is ~ 10 µm) encapsulated with/without MNPs were placed in the center of magnetic-field generator. Steady-state fluorescence of released CF or Dox was measured with a Fluorescence Spectrometer (PerkinElmer, LS55). The emission fluorescence spectra of CF were recorded between 500 and 650 nm in the corrected spectrum mode with excitation wavelength at 492 nm and 10.0 nm slit, while the excitation wavelength of Dox was set at 488 nm. At least 5 scans were averaged for each spectrum. The total fluorescence intensity of sample solution was measured after the capsules were disrupted using Triton X-100. The release percentage of CF or Dox from MLMs was calculated using below equation:

$$\% \text{ release} = \frac{I_{ML}(t) - I_{ML}(0)}{I_{MAX} - I_{ML}(0)} \times 100 \quad (1)$$

where $I_{ML}(t)$ is fluorescence intensity of released CF or Dox from the treated sample at certain time; $I_{ML}(0)$ is the fluorescence intensity of CF or Dox from the untreated sample (control) at starting point; and I_{MAX} is the maximum fluorescence intensity after the same amount of MLMs rupture by the addition of Triton X-100.

2.3 Finite Element Analysis of Magnetic Heating Effect and Magnetic Oscillation of MLMs

Magnetic field distribution is simulated using magnetic field submodule of AC/DC module of COMSOL Multiphysics 4.3. Magnetic heating effect caused by MNPs is simulated using heat transfer/conjugate heat transfer module and magnetic induction heating module of COMSOL Multiphysics 4.3. In the simulation, the magnetic field distribution in the defined space（in quasi-static field）is given by below equations.

$$(i\omega\sigma - \omega^2\varepsilon_0\varepsilon_r)\vec{A} + \nabla \times (\mu_0^{-1}\mu_r^{-1}\vec{B}) = \vec{J}_e \quad (2)$$

$$\vec{B} = \nabla \times \vec{A} \quad (3)$$

$$\vec{J}_e = \frac{NI_{coil}}{S_0}\vec{e}_{coil} \quad (4)$$

Where ω is angular frequency ($\omega = 2\pi f$, f is frequency)；σ is the conductivity of copper (5.998×10^7 S/m)；ε_0 is the vacuum permittivity (8.854×10^{-12} F/m); ε_r is the relative permittivity(1); $\vec{A}$ is magnetic vector potential; μ_0 is the vacuum permeability ($4\pi \times 10^{-7}$ H/m); μ_r is the relative permeability(2300); $\vec{B}$ is magnetic induction intensity and is considered as uniform in a small region; $\vec{J}_e$ is the externally applied current density; N is the turns of coil; I is the current in the coils; S_0 is the cross section area of coil; $\vec{e}_{coil}$ is the direction of current. Boundary condition of the system is considered as magnetically insulation, i.e., $\vec{n} \times \vec{A} = 0$, where $\vec{n}$ is normal vector of boundary. In magneto-calorific simulation, ignoring the fluid convection in this temperature range, the differential equations of heat are given below.

$$\rho C_p(\frac{\partial T}{\partial t} + \vec{u} \cdot \nabla T) = \nabla \cdot (k_B \nabla T) + Q_f \quad (5)$$

$$Q_f = \phi P = \mu_0\chi_0\phi H_m^2 f \frac{2\pi f\tau}{1 + (2\pi f\tau)^2} \quad (6)^{[31]}$$

Where ρ is the density of materials; $\vec{u}$ is direction vector of temperature gradient; C_p is constant pressure heat capacity of solution (4.18J/g $\cdot$℃); T is absolute temperature; k_B is Boltzmann constant (1.38×10^{-23}); Q_f is magnetic heat of MNPs in an AC magnetic field; ϕ is the volume ratio of these MNPs and equivalent total water (0.0024 in this case); P is the volumetric power dissipation; χ_0 is equilibrium susceptibility; H_m is magnetic field intensity; τ is the relaxation time; expression of $\nabla \cdot (k_B \nabla T)$ is the internal energy of system; expression of $\rho C_p (\frac{\partial T}{\partial t} + \vec{u} \cdot \nabla T)$ is the energy of system thermal conduction. Boundary condition of contact surface between water and air is considered as third boundary condition i.e., $-\lambda \frac{\partial T}{\partial n}\big|_s = h(T_s - T_f)$, where λ is material conductivity of water (0.54 W/m K); h is convective heat transfer coefficient; T_s is temperature in interface of LMs and external water; T_f is temperature of the interface between water and external air. Boundary condition of air is considered as first boundary condition *i.e.*, $T_0 = T_{amb} = 293.15$ ℃ , where T_0 is temperature of air boundary; T_{amb} is temperature of external environment. All simulations were finished with a triangular grid meshing. The mesh was adjusted according to local structure to obtain the required convergence at a reasonable computing time scale while maintaining the required accuracy. There were 2.7×10^5 triangular elements involved in the simulation. The input parameters are listed in Supporting Information Table S1. The magnetic field intensity generated was measured using a Teslameter (WT20C, China). The magnetic oscillation in the system shows the magnetic moment swing of MNPs and it mainly relates to three kinds of torque acting on the particle at the same time i.e., magnetic torque $\vec{T}_m$, hydrodynamic torque $\vec{T}_h$, and Brownian torque $\vec{T}_B$.[32] Because of the superparamagnetic property of the MNPs in the experiments, the magnetic torque $\vec{T}_m$ can be expressed as $\vec{m}$ (magnetic moment) multiplied by $\vec{B}$ (the magnetic induction intensity). m is the material saturation magnetization multiplied by the magnetic core volume $M_s V_{core}$. The hydrodynamic torque $\vec{T}_h$ is proportional to the angular velocity of the nanoparticles with magnitude given by the Stokes-Einstein relation for small Reynold's number particles.[32] $\vec{T}_h = -6\eta V_{hyd} \vec{\Omega}$, where $\vec{\Omega}$ is angular velocity, V_{hyd} is the hydrodynamic volume of the particle, and η is the fluid's viscosity. $\vec{T}_B$ is the fluctuating torque generated by the Brownian movement of nanoparticles themselves.[32] The actual magnetic nanoparticles in our experiment meet the Reynold number condition, so the inertia can be neglected. The complete balance of torques considering all factors can be expressed as follows: [32, 33]

$$\vec{T}_m + \vec{T}_h + \vec{T}_B = 0 \quad (7)$$

In the case of an external oscillating magnetic field, $H = H_0 \cos(2\pi ft) \vec{i}_z$, the dipole moment of the particles follows the oscillations of the magnetic field with a phase-lag between the field and the particle. The z-component of the magnetization (the solution of equation (7)) $\vec{m}_z$ can be got from the equation (7) and can be expressed as: [32, 34]

$$\vec{m}_z = \frac{1}{3}\alpha[\chi'\cos(2\pi ft) + \chi''\sin(2\pi ft)]\vec{i}_z \quad (8)$$

where $\alpha = mB / k_B T$ is the parameter in Langevin function and is directly related to the magnitude of magnetic field. χ' and χ'' are the in-phase and out-of-phase of susceptibility respectively and

are given as : $\chi' = \dfrac{\chi_0}{1 + (2\pi f \tau_B)^2}$, and $\chi'' = \dfrac{\chi_0 (2\pi f \tau_B)}{1 + (2\pi f \tau_B)^2}$. [35]

$\tau_B = \dfrac{3\eta V_{hyd}}{k_B T}$ is the Brownian relaxation time. We define $\vec{n}$ to be the unit vector firmly attached to the particle. For a moderate magnetic field, the z-component of the particle has a relationship with $\vec{m}_z$ and can be expressed as below: [33]

$$\vec{n}_z = \vec{m}_z - G\frac{\partial \vec{m}_z}{\partial t} = \left[\left(\frac{1}{3}\alpha\chi' + \frac{2}{3}\alpha\pi fG\chi''\right)\cos(2\pi ft) + \left(\frac{1}{3}\alpha\chi'' - \frac{2}{3}\alpha\pi fG\chi'\right)\sin(2\pi ft)\right]\vec{i}_z$$

$$(9)$$

where $G = K_1 / 3\eta$ is a coefficient related to the property of magnetic nanoparticle rather than the particle radius. The maximum value (modulus) of $\vec{n}_z$, $\dfrac{1}{3}\alpha\sqrt{\dfrac{1 + (2\pi fG)^2}{1 + (2\pi f \tau_B)^2}}$, is frequency dependent.

2.4 Cell-Culture and Cell Viability Measurements

HeLa cells were purchased from ATCC and cultured under recommended conditions. To be specific, they were cultured in RPMI 1640 medium supplemented with 10% FBS (heat-inactivated) in a 5% CO_2 atmosphere at 37℃ . Then the cells were separated from the medium by centrifugation at 1000 rpm for 3 min and washed three times with a sterile PBS solution (pH 7.2) after culturing for 2 days. A homogeneous cell suspension was obtained by redispersing the cell sediment in the 1640 cell culture medium. The cell number was determined using a cell counting chamber. These cells (1×10^4) were mixed with LMs loaded with Dox (4.2×10^7 Dox/LMs) and cultured in 96-well plates for 24 h, whereas the control groups were cultured without LMs. The 3-(4,5-dimethylthiazol-2-yl)-2,5-diphenyltetrazolium (MTT) (Sigma Inc.) assay was carried out following standard protocol to determine the relative cell viabilities with different treatments. Stained cells were observed at 10×20 magnification using a fluorescence microscope (Nikno 80i, Japan).

3 Results and Discussion

3.1 Synthesis of the Magnetic CF (or drug) loaded LMs

MNPs prepared by co-precipitation method have the preferable water-solubility and size-controllability. The morphology of these nanoparticles was characterized by TEM as shown in Fig. S2a. The diameters of citrate-coated nanoparticles and APTES-coated nanoparticles are 10.2±2.1 nm and 12.0±2.3 nm respectively. The surface functional groups of MNPs were confirmed by FTIR spectra (Fig. S2b). There are carboxyl (COOH) groups on citrate-coated nanoparticles and amino (NH_2) groups on APTES-coated nanoparticles. Zeta potential measurements of these nanoparticles show the zeta potentials of citrate-coated nanoparticles to be -34.5 mV and amino-coated MNPs to be 34.1 mV. The crystal structure of products was also studied by X-ray powder diffraction (XRD) technique (Fig. S2c). The positions of diffraction peaks are assigned to the crystal faces of a cubic-phase Fe_3O_4.[36] According to Debye-Scherrer equation, the sizes of deposited Fe_3O_4 crystallite of carboxyl-coated nanoparticles and amino-coated nanoparticles were evaluated to be 9.1 nm and

12.1 nm, respectively, which are in good agreement with those from TEM statistical results. The room-temperature hysteresis loops of these Fe_3O_4 nanoparticles were measured using a vibrating sample magnetometer (VSM) (Fig. S2d). The magnetic saturation value was 62.8 emu/g for carboxyl nanoparticles and 60.7 emu/g for amino nanoparticles, respectively. No remanence or coercivity was detected in the magnetic hysteresis loops of room temperature. The superparamagnetic character of these MNPs is very important for heat generation in AMF irradiation.[37]

MLMs loaded with CF (or Dox) were prepared by electro-formation method.[28] MNPs and CF (or Dox) were dissolved together in water as solution medium for lipid microcapsules formation. The formed MLMs were purified by filtering before release experiments in order to get rid of the particles and CF (or Dox) outside of the MLMs, the size distribution of these MLMs was ploted in Fig. S3. Considering the easiness for microscopy observation, MNPs and CF (or Dox) were also dissolved in 0.20 M sucrose solution. MLMs were then diluted 30 times with an iso-osmolar solution of 0.20 M glucose. The density difference between sucrose (inside the capsules) and glucose (outside) leads to MLMs sinking to the slide surface, which is good for microscopy observation. These MLMs respond to an external magnetic field. Fig. S4a shows the images of DOPC MLMs encapsulated with carboxyl MNPs. The magnetic DOPC LMs move along the direction of external magnetic field. MNPs inside microcapsules were also arranged into lines as indicated by white arrows in the left image of Fig. S4a. Upon stopping the external magnetic field, MLMs stop moving and the nanoparticles lines inside the microcapsules dispersed again as indicated by white arrows in the right image of Fig. S4a. The loading amount of nanoparticles can be adjusted by varying the initial concentration of nanoparticles. Zeta potentials of these MLMs (-7.8 mV) and CF loaded MLMs (-7.6 mV) are almost equal to the pure LMs labeled with 0.5% TR-DHPE (red, negative), which indicates that the carboxyl MNPs (charged negatively) was encapsulated into LMs. In contrast, amino MNPs were adsorbed onto the LMs surface rather than encapsulated inside the LMs mainly because of the electrostatic interactions. The nanoparticles adsorbed on surface make these LMs look like strawberry appearance, and these MNPs did not arrange or move freely (white arrows in Fig. S4b). These MLMs move or rotate as a whole in external magnetic fields. The SEM and AFM images of these MLMs were shown in Fig. S5. The Zeta potentials of amino MNP modified MLMs and Dox loaded MNPs were measured to be 26.6 mV and 24.2 mV respectively, which also confirmed the amino MNPs are on the surface of LMs.[11]

3.2 CF and Dox Release from MLMs under Different AMF

After non-encapsulated/adsorbed nanoparticles and drug outside LMs were filtered away by polycarbonate membranes, the sample solution was put in the centre of magnetic field coils and a water circulation jacket was supplied to control the environmental temperature and insulate the thermal effect from the induction coil. Alternate magnetic field (AMF) with different parameters was applied to trigger the drug release. The magnetic fluorescence LMs were clearly seen under microscope for observation of the release process triggered by AMF. Fig. 2a is the fluorescence images of DPPC LMs loaded with CF and

carboxyl MNPs as a function of time without applying AMF. The green core is the CF solution, while the red ring indicates the lipid bilayers. After 20 minutes, CF was not released out from the LMs. However, the green color became faint against time upon applying AMF (2 kHz, 20 mT) as shown in Fig. 2b, which indicated the release of CF from MLMs. The release of CF (or Dox) was influenced by magnetic field, exposure time and concentration of MNPs. We used the Fe element concentration to represent the concentration of MNPs in following experiments. In the following contents, the influences of magnetic field frequency and Fe concentration on CF (or Dox) release of magnetic DPPC LMs were studied with 5 minutes interval AMF (20 mT), as shown in Fig. 2. When the Fe concentration and the AMF strength were fixed to be 21.1 μg/mL and 20 mT, the CF release behavior at frequency of 500 Hz (red), 2 kHz (blue) and 5 kHz (green) were plotted as shown in Fig. 2c. The light green and pink backgrounds represent AMF state of "on" and "off" respectively. The CF release of each given parameter was carried out at least 3 times. It is noted that the CF release synchronizes with the AC magnetic field switch very well. For each frequency, the release speed of CF is greater in early stage than later stage although applying the same period of AMF. Release percentage increases gradually with trigger cycles, and levels off afterwards. The release percentage increases with increasing frequency. According to magnetocaloric theory, frequency is the main factor of magnetic heating. Higher frequency generates greater thermal energy to heat the solution, which destabilizes the lipid bilayer and causes the out-leaking of intraliposomal contents.[38] The maximum release percentage can be up to about 70 % at frequency of 5 kHz with Fe concentration 21.1 μg/mL. Fig. 2d shows the CF release behavior at Fe concentration of 10.5 μg/mL (red), 21.1μg/mL (blue), and 42.2 μg/mL (green) with frequency of 2 kHz. The higher concentration of Fe results higher release percentage. More MNPs generate greater heat to drive CF release. Effect of Fe concentrations on CF release is relative small comparing with frequency. Considering the bio-security of external materials in actual treatment, we use low Fe concentration in the premise of high release percentage. Fe concentration of 21.1 μg/mL was used for CF release experiments with different frequency. The release efficiency of our system is comparable to or greater than the report in same amount of Fe.[39] In particular, the CF slowly released during the initial two minutes after applying AMF, but released rapidly afterwards, as shown in the inserts of Fig. 2c and d. The phase transition temperature (Tm) of DPPC is 41℃, so it was in gel phase at room temperature. It took a bit time to heat up DPPC from gel phase to liquid crystal phase. When the temperature was higher than the Tm of DPPC, CF released quickly. At the "off" stage, CF release slowed down. The increase of release percentage become less as increasing the trigger cycle because of the less concentration gradient of CF between inside and outside of MLMs. If the AMF was applied continuously, CF release percentage was higher than that by applying the pulse AMF with same period. There was almost no CF release from the MLMs without external magnetic field, as shown by black plots in Fig. 2. The magnetic field trigger is important and necessary for intra content release. When the same experimental protocol was applied to the CF LMs samples without MNPs, almost no CF release was detected. Therefore, AMF exposure has no effect on release property of LMs without MNPs.

Journal of Materials Chemistry B

PAPER
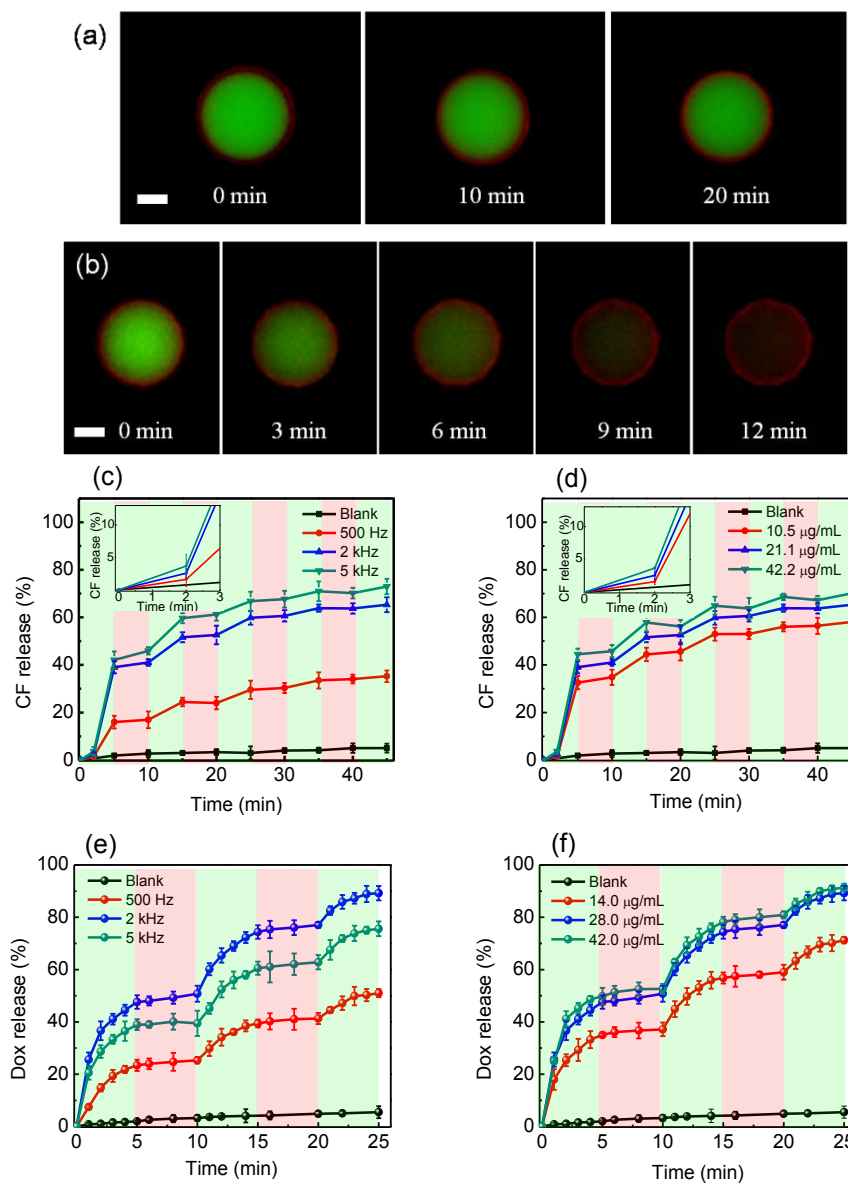
Fig.2 Fluorescence images of DPPC MLMs loaded with CF and carboxyl MNPs as a function of time (a) without AMF (control) and (b) upon applying AMF (2 kHz, 20mT). These images were obtained by merging the images from FITC channel (for CF) and rhodamine channel (for TR-DHPE). Scale bar are 10 μm in all images. (c) CF release behavior of CF-loaded magnetic (carboxyl MNPs) DPPC LMs at frequency of 500 Hz (red), 2 kHz (blue) and 5 kHz (green) respectively, at Fe concentration of 21.1 μg/mL. The insert is zoom-in view of the first 3 minutes. (d) CF Release behavior of CF-loaded magnetic (carboxyl MNPs) DPPC LMs at Fe concentration of 10.5 μg/mL (red), 21.1 μg/mL (blue), and 42.2 μg/mL (green) respectively at frequency of 2 kHz. The insert is zoom-in view of the first 3 minutes. (e) Dox release behavior of Dox-loaded magnetic (amino MNPs) DPPC LMs at frequency of 500 Hz (red), 2 kHz (blue) and 5 kHz (green) respectively, at Fe concentration of 28.0 μg/mL. (f) Dox release behavior of Dox-loaded magnetic (amino MNPs) DPPC LMs at Fe concentration of 14.0 μg/mL, 28.0 μg/mL, and 42.0 μg/mL respectively, at a frequency of 2 kHz. The interval of AMF trigger is 5 minutes. The light green and pink background represents the AMF at the state of "on" and "off" respectively. The black curves were obtained without applying AMF as controls. The error bars are based on the standard deviation (SD) of three samples

Because the magnetic microcapsules aims for medical application, the Dox (anti cancer drug) release behavior was investigated. Since the Tm of DPPC is only several degree higher than the body temperature, thermo sensitive DPPC LMs are designed as the carrier for Dox. All dynamic Dox release experiments were performed at room temperature. The amino MNPs with different concentration were mixed with Dox as solution medium to prepare MLMs. In this case the MNPs were adsorbed on the surface of LMs. The fluorescence images of Dox loaded DPPC MLMs as a function of time without and with applying AMF were shown in Fig. S6. Effects of AMF frequency and Fe concentration on Dox release behavior were investigated in details as shown in Fig. 2e and f respectively. It can be seen that the overall trend of intra Dox release pattern is similar to that of CF releasing. The Dox release synchronized with the AC magnetic field on/off very well with a stepped release percentage increase. Contrast to the CF release behavior of carboxyl MNPs loaded LMs, Dox release is peaked at a frequency of 2 kHz. The maximum release percentage is up to about 90 % at 25 minutes. Although the Dox release increases with increasing concentration of amino MNPs in the preparation medium, the difference between 28.0 and 42.0 μg/mL is very small. As mentioned in the above section, amino MNPs adsorb on the surface rather than inside LMs, there is limited superficial area for nanoparticle adsorption. According to our calculation, the average number of amino MNPs around one microcapsule is 2.181×10^6 in theory. The actual amount of adsorbed MNPs per LMs is 1.597×10^6 from TGA analysis (Fig. S7), which indicates LMs are almost fully covered by MNPs. The most important thing to note is that there is no lag period as observed for carboxyl MNPs MLMs, i.e., Dox release started immediately after applying AMF, which implied that both magnetic oscillation and magnetic-heating contributed the release of Dox.[39]

3.3 Finite Element Analysis of Magnetic Field Heating and Magnetic oscillation

The simulations were done to investigate the releasing behavior difference between carboxyl and amino MNP LMs. Two main factors, i.e. magnetic heating and magnetic oscillation, from MNPs in AMF are proposed to respond for the release behavior of MLMs. A simulation result of magnetic field distribution is shown in Fig. S8. The simulations are based on actual experimental conditions, and the actual measured value was consistent with the simulation results. The temperature of these two sample solution obtained from simulation is plotted as a function of time at different frequency, as shown in Fig. 3a, b, respectively. It is noted that the temperature of these two systems increases with increasing frequency from 500 Hz to 5 kHz. There is almost no temperature increasing at frequency of 50 Hz, which means that there are no obvious magnetic losses at low frequency. The simulation results fit with the theory of relaxation losses dissipation equation.[40, 41] The nanoparticle oscillation also

occurs upon applying AMF. The magnetic oscillation amplitudes of MNPs in aqueous pool and adsorbed on the surface were calculated using the equation (9) and shown in Fig. 3c. All calculations were based on the actual size of MNPs used in the experiments. For the amino MNP system, the effective amplitude is 1.0 at frequency range less than 10^2 Hz, and is 0 at frequency range over 10^5 Hz, while it gradually decreases between 10^2 and 10^5 Hz. But the magnetic oscillation frequency of carboxyl MNP system shifts to higher frequency because of their free diffusion in the solution. We believe that for carboxyl MNP LMs the magnetic heating plays dominate role on drug release, because negatively charged MNPs were away from the lipid bilayer due to the electrostatic repulsion and magnetic oscillation occurs inside the LMs, which is no influence on drug release. From Fig. 3a, it is noted that at 2 minutes the solution temperature is 51℃, 72℃ and 74℃ for 500 Hz, 2 kHz, and 5 kHz respectively, which explains the result of 2 minutes lag in the inset of Fig. 2c. The higher frequency results in higher temperature, which is matching the results of more CF release from higher frequency in Fig. 2c. As to the system of the amino MNP LMs, both magnetic heating and magnetic oscillation play roles for drug release. The oscillation of nanoparticles on the membrane surface causes temporary holes for out-leaking of intraliposomal Dox when AMF is applied; meanwhile magnetic heat (41℃, 42℃ and 42℃ degree at 2 minutes for 500 Hz, 2k Hz, and 5k Hz) also accelerates the transformation of lipid bilayer from gel to liquid phase and promotes Dox leakage. The contribution from magnetic oscillation causes release to happen immediately after applying AMF. Although the high frequency leads to more magnetic heat, the strong oscillation at 2 kHz (0.59) compared with relative week oscillation at 5 kHz (0.28) causes greater release at 2 kHz than that at 5 kHz, which explains the results in Fig. 2e. It is the synergistic results of magnetic heat and magnetic oscillation for out-leaking of intraliposomal Dox in the amino MLMs. The release efficiency of LMs with MNPs on their surfaces is much higher than that of LMs containing MNPs in their lumens.

3.4 In vitro Cell Viability Experiments

The in vitro cytotoxicity of different treatment on HeLa cells using magnetic responsible LMs was estimated by the 3-(4,5-dimethylthiazol-2-yl)-2,5-diphenyltetrazo-lium bromide (MTT) assay (Fig. 4a).[42] Data of normalized mean and standard error of each test were obtained from three independent experiments. It can be seen that there is almost no cytotoxicity of magnetic field (treatment 2) and carrier itself (treatment 3) toward HeLa cells. Cell viability decreases 10 % when treated with the MLMs without Dox loading upon applying AMF of 2 kHz for 5 min (treatment 4). So magnetic heat and magnetic oscillation of MNPs themselves have little influence on cells growth because these carriers were not endocytosed easily by normal cancer cells.
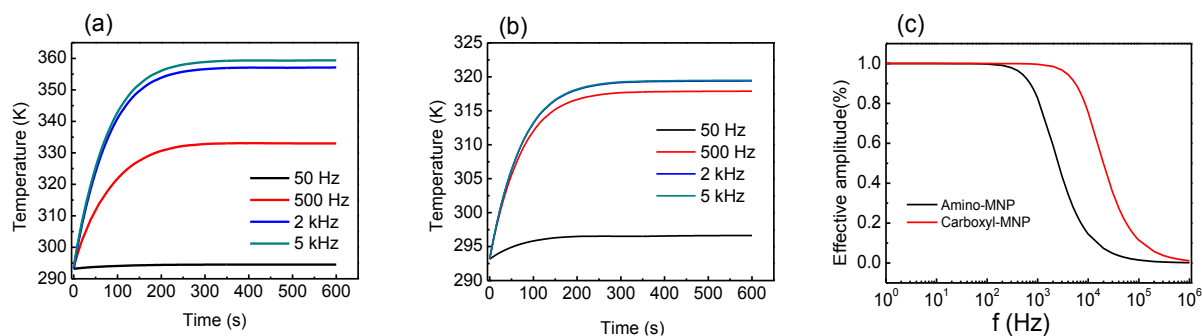
Fig. 3 (a) and (b) are the simulated temperature curves of carboxyl MNP and amino MNP at different frequencies at Fe concentration of 21.1 μg/mL. (c) Magnetic oscillation curve of carboxyl MNP and amino MNPs as a function of frequency.
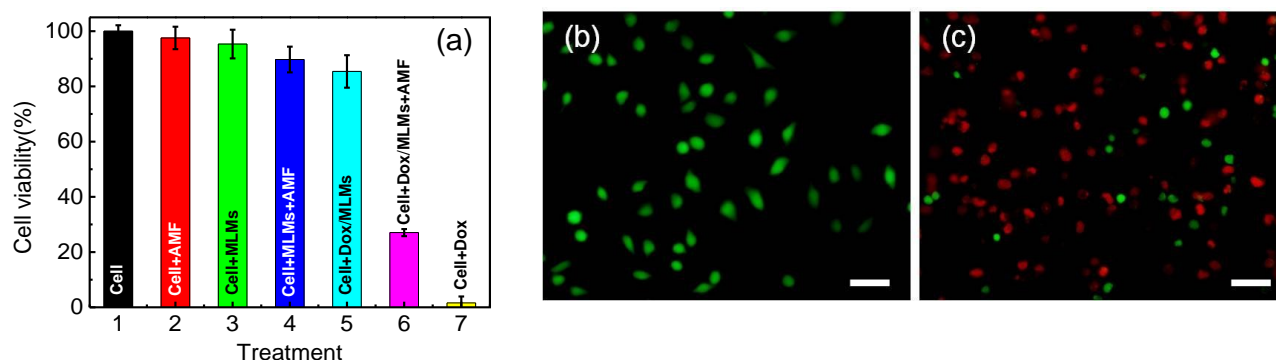
Fig.4 In vitro cytotoxicity of HeLa cells. (a) Cell viability of different treatments was measured by MTT assays after 24 h incubation at 37 ℃. Data show the normalized mean and standard error of three independent experiments, each performed in triplicate. (b) and (c) are the fluorescence microscopy images of HeLa cells of control and experiment group after incubation for 24 h at 37 ℃ with AMF of 2 kHz for 5min. Scale bar is 50 μm.

Similar cell viability was obtained when the cells were incubated with amino MNPs Dox loaded LMs without AMF trigger （treatment 5), which may be caused by the leakage of Dox naturally. However it shows very obvious cytotoxicity when they are triggered by AMF (2 kHz, 5 min) treatment (treatment 6, Dox concentration 4.0 μg/mL).The viability of the cells was about less than 30 % at 5 min exposure time of 2 kHz for 24 h incubation time, which is superior to the efficiency of other drug carries.[42] While almost 100% HeLa cells died at this concentration using pure Dox directly. It demonstrates that Dox was effectively released by the trigger of AMF and the better therapeutic efficiency mainly depends on the released drug but not the endocytosed carriers. Significantly enhanced cytotoxicity was observed as incubation time increased. When the incubation time extended to 48 h, nearly 100% HeLa cells died. At same time, cell viability decreases with increasing payload concentration (Fig. S9). Fig. 4b and c are the fluorescence microscopy images of HeLa cells incubated without and with MLMs containing 4.0 μg/mL Dox concentration for 24 h. Living cells were stained by calcein-AM showing green color while dead cells were stained by PI showing red color. From the percentage of dead cells in control (Fig. 4b) and experiment groups (Fig. 4c), it is easy to see that the method proposed here is very effective to promote tumour cell apoptosis.

4. Conclusions

In this work, two types of magnetic lipid microcapsules (MLMs) are fabricated, i.e., MLMs with carboxyl MNPs inside and MLMs with amino MNPs on their surfaces. We demonstrated that different charged MNPs were encapsulated into the aqueous pool or absorbed on surface of these lipid microcapsules (LMs). Using the magnetic heat effect and magnetic oscillation of MNPs in a non-invasively AMF, CF and Dox releasing from LMs in these two different systems were investigated at 5 minutes intervals. The releases percentage of these two types MLMs increased with increasing Fe concentration. The release percentage increases against frequency for MLMs system with MNPs inside; while it peaks at 2 kHz for MLMs system with MNPs adsorbed on their surfaces. The release rate is quicker in the initial few minutes for amino MNP modified MLMs. Although the intra drug release of these two types MLMs are all both synchronized with the AMF switch very well, the different mechanisms were discussed on the basis of the simulation and experimental results. Magnetic heat and magnetic oscillation of MNPs in AMF are the main factor for loading drug release. We believe that for carboxyl MNP LMs the magnetic heating plays dominate role on drug release, because negatively charged MNPs were away from the lipid bilayer

due to the electrostatic repulsion and magnetic oscillation occurs inside the LMs. As to the system of the amino MNP LMs, both magnetic heating and magnetic oscillation play roles for drug release. The oscillation of nanoparticles on the membrane surface causes temporary holes for out-leaking of intraliposomal Dox when AMF is applied. It is the synergistic results of magnetic heat and magnetic oscillation for out-leaking of intraliposomal Dox. The release efficiency of MLMs with MNPs on their surfaces is much higher than that of MLMs containing MNPs in their lumens. The *in vitro* cytotoxicity results of Dox loaded MLMs against HeLa cells show that the controlled release of these carries are effective in the level of cells. It has great potential in targeted and controlled drug delivery in cancer treatment.

Acknowledgements

References

1 E. Fleige, M. A. Quadir, R. Haag, *Adv. Drug. Deliver. Rev.* **2012**, *64*, 866-884.

2 B. P. Timko, T. Dvir, D. S. Kohane, *Adv. Mater.* **2010**, *22*, 4925-4943.

3 S. A. Dergunov, J. Durbin, S. Pattanaik, E. Pinkhassik, *J. Am. Chem. Soc.* **2013**, *136*, 2212-2215.

4 K. E. Broaders, S. J. Pastine, S. Grandhe, J. M. J. Frechet, *Chem. Commun.* **2011**, *47*, 665-667.

5 R. Casasus, E. Climent, M. D. Marcos, R. Martinez-Manez, F. Sancenon, J. Soto, P. Amoros, J. Cano, E. Ruiz, *J. Am. Chem. Soc.* **2008**, *130*, 1903-1917.

6 S. V. Aathimanikandan, E. N. Savariar, S. Thayumanavan, *J. Am. Chem. Soc.* **2005**, *127*, 14922-14929.

7 H. Kim, D. Lee, J. Kim, T.-i. Kim, W. J. Kim, *ACS Nano* **2013**, *7*, 6735-6746.

8 C. Park, J. Lim, M. Yun, C. Kim, *Angew. Chem. Int. Edi.* **2008**, *47*, 2959-2963.

9 M. Ochs, S. Carregal-Romero, J. Rejman, K. Braeckmans, S. C. De Smedt, W. J. Parak, *Angew. Chem. Int. Edi.* **2013**, *52*, 695-699.

10 T. Hoare, J. Santamaria, G. F. Goya, S. Irusta, D. Lin, S. Lau, R. Padera, R. Langer, D. S. Kohane, *Nano Letters* **2009**, *9*, 3651-3657.

11 S. Carregal-Romero, P. Guardia, X. Yu, R. Hartmann, T. Pellegrino, W. J. Parak, *Nanoscale* **2015**, *7*, 570-576.

12 S. Nappini, M. Bonini, F. B. Bombelli, F. Pineider, C. Sangregorio, P. Baglioni, B. Norden, *Soft Matter* **2011**, *7*, 1025-1037.

13 S. L. Huang, *Adv. Drug. Deliver. Rev.* **2008**, *60*, 1167-1176.

14 S. Hernot, A. L. Klibanov, *Adv. Drug. Deliver. Rev.* **2008**, *60*, 1153-1166.

15 M. N. Antipina, G. B. Sukhorukov, *Adv. Drug. Deliver. Rev.* **2011**, *63*, 716-729.

16 R. Tietze, J. Zaloga, H. Unterweger, S. Lyer, R. P. Friedrich, C. Janko, M. Pöttler, S. Dürr, C. Alexiou, *Biochem. Bioph. Res. Co.* **2015**, *468*, 463-470.

17 C. Wang, H. Xu, C. Liang, Y. Liu, Z. Li, G. Yang, L. Cheng, Y. Li, Z. Liu, *ACS Nano* **2013**, *7*, 6782-6795.

18 L. Zhou, B. He, F. Zhang, *ACS Appl. Mater. Inter.* **2012**, *4*, 192-199.

19 T. Hoare, B. P. Timko, J. Santamaria, G. F. Goya, S. Irusta, S. Lau, C. F. Stefanescu, D. Lin, R. Langer, D. S. Kohane, *Nano Lett.* **2011**, *11*, 1395-1400.

20 X. Chen, R. Klingeler, M. Kath, A. A. El Gendy, K. Cendrowski, R. J. Kalenczuk, E. Borowiak-Palen, *ACS Appl. Mater. Inter.* **2012**, *4*, 2303-2309.

21 A. Baeza, E. Guisasola, E. Ruiz-Hernández, M. Vallet-Regí, *Chem. Mater.* **2012**, *24*, 517-524.

22 S. Kondaveeti, D. R. Cornejo, D. F. Petri, *Colloid. Surfaces B.* **2016**, *138*, 94-101.

23 Y. Chen, A. Bose, G. D. Bothun, *ACS Nano* **2010**, *4*, 3215-3321.

24 E. Amstad, J. Kohlbrecher, E. Müller, T. Schweizer, M. Textor, E. Reimhult, *Nano Letters* **2011**, *11*, 1664-1670.

25 Y. I. Golovin, S. L. Gribanovsky, D. Y. Golovin, N. L. Klyachko, A. G. Majouga, A. M. Master, M. Sokolsky, A. V. Kabanov, *J. Control Release.* **2015**, *219*, 43-60.

26 A. K. Hauser, R. J. Wydra, N. A. Stocke, K. W. Anderson, J. Z. Hilt, *J. Control Release.* **2015**, *219*, 76-94.

27 W. Aadinath, T. Ghosh, C. Anandharamakrishnan, *J. Magn. Magn. Mater.* **2016**, *401*, 1159-1172.

28 M. I. Angelova, D. S. Dimitrov, *Faraday Discuss* **1986**, *81*, 303-311.

29 K. S. Horger, D. J. Estes, R. Capone, M. Mayer, *J. Am. Chem. Soc.* **2009**, *131*, 1810-1819.

30 H. Bi, B. Yang, L. Wang, W. Cao, X. Han, *J. Mater. Chem. A* **2013**, *1*, 7125-7130.

31 C. L. Ondeck, A. H. Habib, P. Ohodnicki, K. Miller, C. A. Sawyer, P. Chaudhary, M. E. McHenry, *J. Appl. Phys.* **2009**, *105*. 07B324.

32 N. A. Usov, B. Y. Liubimov, *J. Appl. Phys.* **2012**, *112*. 23901.

33 D. B. Reeves, J. B. Weaver, *J. Appl. Phys.* **2012**, *112*, 124311.

34 J. H. Sanchez, C. Rinaldi, *J. Magn. Magn. Mater.* **2009**, *321*, 2985-2991.

35 B. Wang, C. Xu, J. Xie, Z. Yang, S. Sun, *J. Am. Chem. Soc.* **2008**, *130*, 14436-11437.

36 L. Serra, J. Domenech, N. A. Peppas, *Biomaterials* **2006**, *27*, 5440-5451.

37 T. Neuberger, B. Schopf, H. Hofmann, M. Hofmann, B. von Rechenberg, *J. Magn. Magn. Mater.* **2005**, 293, 483-496.

38 E. Amstad, E. Reimhult, *Nanomedicine.* **2012**, 7, 145-164.

39 A. Diguet, M. Yanagisawa, Y. J. Liu, E. Brun, S. Abadie, S. Rudiuk, D. Baigl, *J. Am. Chem. Soc.* **2012**, *134*, 4898-4904.

40 A. H. Habib, C. L. Ondeck, P. Chaudhary, M. R. Bockstaller, M. E. McHenry, *J. Appl. Phys.* **2008**, *103*. 07A307.

41 R. E. Rosensweig, *J. Magn. Magn. Mater.* **2011**, *323*, 1191-1197.

42 Y. Zhu, J. Shi, W. Shen, X. Dong, J. Feng, M. Ruan, Y. Li, *Angew. Chem. Int. Edi.* **2005**, *44*, 5083-5087.

A graphical and textual abstract
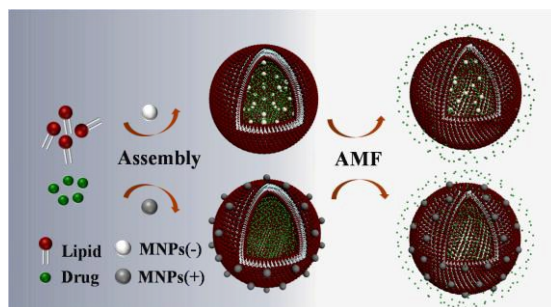
The drug release of two types MLMs both synchronize the AMF switch, the different mechanisms were discussed in this paper